Intermittent Turbulence and Oscillations in the Stable Boundary Layer over Land. Part I: A Bulk Model

B. J. H. Van de Wiel, R. J. Ronda, A. F. Moene, H. A. R. De Bruin, and A. A. M. Holtslag

Department of Meteorology and Air Quality, Wageningen University, Wageningen, Netherlands

ABSTRACT

In the stable boundary layer (SBL) it is observed often that turbulence is not continuous in space and time. This discontinuous, intermittent turbulence causes alternations from the mean evolution of the stratified atmospheric boundary layer, which may result in an oscillatory type of behavior of the near-surface wind speed and temperature. It is well known that intermittent turbulence in the SBL can be generated by various mechanisms.

This paper focuses on an intermittency generating mechanism that arises from a direct interaction of the lower atmosphere (first tens of meters) with the vegetation surface, without interaction with the air aloft. It is shown that the essence of this mechanism can be captured by a 1D bulk model of three coupled nonlinear differential equations.

In the present paper, numerical runs with the model show that intermittent turbulence is most likely to occur over land surfaces with low vegetation during clear-sky conditions in the presence of a moderate to low synoptical pressure gradient. The existence of a vegetation layer has a strong influence on intermittency dynamics. Due to its small heat capacity, the vegetation temperature is able to quickly respond to rapidly changing conditions. This in turn affects the stability of the lower atmosphere, causing an important feedback mechanism.

In addition, it was found that intermittent behavior of SBL models occurs for various first-order closure schemes with different stability functions. However, stability functions that allow turbulent transport beyond the critical Richardson number effectively suppress intermittent–oscillatory behavior. Currently, the latter type of formulations is often used in numerical weather prediction to prevent excessive SBL cooling in very stable conditions.

The advantage of using a simplified SBL model, as proposed in the present paper, is that it allows an analytical study of the system, which, in turn, allows theoretical predictions about the occurrence of intermittent SBL behavior (see the companion paper).

1. Introduction

On clear nights with weak winds, a frequently observed phenomenon is the weak and intermittent character of turbulence. Intermittent turbulence is characterized by brief episodes of turbulence with intervening periods of relatively weak or unmeasurable small fluctuations (Mahrt 1999). In this study we indicate intermittency by so-called "global intermittency" in a sense that, in the periods of weak turbulence, eddies on *all* scales are missing of suppressed. This type of intermittency differs from the so-called "fine-scale intermittency," sometimes found in turbulence literature, where fine-scale structures occur intermittently within larger eddies (Mahrt 1989).

An example of this global intermittency is given in Fig. 1. Figure 1 shows the development of the turbulent heat flux near the surface during a clear night with relatively weak winds. The measurements were obtained from sonic measurements (5-min averages) of the Wageningen Meteorology and Air Quality group during the 1999 Cooperative Atmosphere Surface Exchange Study (CASES99) field campaign (for a general description of this experiment see Poulos et al. 2000). The example shows a clear alternation between strongly turbulent periods with large negative heat fluxes and more quiet periods with hardly any heat flux. The discontinuous, intermittent turbulence causes changes in the mean evolution of the near-surface temperature and wind speed. In cases when the period of the intermittent turbulence is regular, this may result in oscillatory behavior of the mean quantities. Therefore, in this text both "oscillatory behavior" and "intermittency" refer to the same phenomenon.

For comparison, the results of a clear night with strong winds are shown, obtained during the same campaign. A totally different behavior is visible with continuous turbulence resulting in an almost constant turbulent heat flux during the night. This type of weakly stratified cases is often found during nights with strong winds and/or during nights with cloudy conditions.

Corresponding author address: Dr. B. J. H. Van de Wiel, Department of Meteorology and Air Quality, Duivendaal 2, Wageningen University, Wageningen 6701 AP, Netherlands.
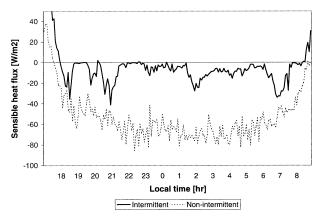E-mail: Bas.vandewiel@user.metair.wau.nl

FIG. 1. Observed turbulent heat fluxes on two clear nights of 14–15 and 17–18 Oct 1999, during the CASES99 field experiment, in KS. The thick line represents a case with discontinuous turbulence (i.e., globally intermittent), observed in conditions with light surface winds. The dashed line represents a case with continuous turbulence (i.e., not globally intermittent), observed in conditions with strong surface winds.

The knowledge of the physical mechanism(s) behind the intermittent behavior of turbulence in the stable boundary layer (SBL) is still very limited, partly because of difficulties in measuring fluxes in weak, intermittent turbulence. It is unclear whether intermittency is generated by local shear effects, by instability on the scale of the entire surface inversion layer or by turbulence generated aloft diffusing to the surface [see review on SBL issues by Mahrt (1999)]. Also, locally produced waves formed by Kelvin–Helmholtz instabilities could play a role in triggering turbulence bursts [e.g., Nappo 1991; also recently observed during CASES99 by Blumen (2001, personal communication)] as could the transverse eddies produced by the inflection point mechanism (Thorpe and Guymer 1977).

In this study we focus on an intermittency mechanism which results from a delicate interplay between radiative cooling and turbulent mixing in presence of a pressure gradient. This mechanism can be described as follows (cf. Businger 1973): On clear nights thermal stability may increase fast, compared to the existing wind shear, due to the strong cooling of the surface. As a consequence the gradient Richardson number increases considerably and therefore turbulence is suppressed and, eventually, collapses. This results in a decoupling of the air from the surface. At this point, due to the very little friction acting on the air, the omnipresent pressure force starts to accelerate the air mass. Thus, shear increases until $Ri < Ri_{crit}$, eventually regenerating turbulence. As a result of this turbulence both stratification and shear are reduced quickly. Due to the strong surface radiation the stratification soon intensifies, causing Ri to increase so that turbulence is suppressed again. Now the whole process starts over again. Several cycles of the behavior sketched above results in an intermittent character of

turbulence in the stable boundary layer and oscillations in the near-surface wind speed and temperature.

At present, it is not clear whether this mechanism generates intermittent turbulence aloft—for example, near the low-level jet (Vukelic and Cuxart 2000; Ha and Mahrt 2001)—or that it generates intermittent turbulence near the surface via a direct surface–atmosphere interaction (Revelle 1993). In this study we confine ourselves to the direct interaction of the lower stratified atmosphere (first tens of meters) with the surface, without considering interaction with the atmosphere aloft. The intermittency caused by this interaction is referred to in the following as atmosphere–surface intermittency (ASI).

Following the results of Blackader (1979), Revelle (1993) carried out a numerical study of SBL behavior using a one-dimensional multilayer model. His model uses a simple first-order turbulence closure for the air layers with diffusion coefficients depending on the local gradient Richardson number. The surface energy balance at the soil surface is solved for dry conditions. Even with this simple model, the SBL shows intermittent turbulent behavior near the surface for a certain range of geostrophic wind speeds. Also the intermittent, near-surface dynamics does not show interaction with the developing low-level jet aloft. The period of the intermittent turbulence calculated by the model varies between ½ h to 4 h depending on the actual environmental circumstances. The modeled periods are within the range of experimental results obtained by others as reported in Revelle (1993). Using a fog prediction model with comparable turbulence parameterization, Welch et al. (1986) clearly showed oscillatory behavior in radiation fog, resulting in a series of fog dissipation and redevelopment episodes. The same study also shows oscillatory behavior of fog development in field observations. Note that, an alternative explanation for oscillatory behavior in a particular fog event at Cabauw was given by Duynkerke (1991) in terms of gravity wave theory.

McNider et al. (1995) carried out a theoretical study on SBL dynamics. Although they did not explain the oscillatory behavior of the models mentioned above, their approach using bifurcation techniques applied to a simplified model largely inspired the present work and its companion paper (described below).

An understanding of the physics behind intermittent turbulence and oscillations is of great practical importance for parameterization of the very stable boundary layer for numerical weather prediction (NWP) purposes. It is, for example, easy to understand why the commonly used average flux–profile relationships will be violated in intermittent flows: under these conditions the mean fluxes are largely determined by the (relatively short) bursting period, whereas the mean gradients are largely determined by the longer quiet periods with large gradients. This implies that no universal relationship can be found between the time-averaged profiles and the

mean flux. In practice, however, the effect of intermittent turbulence is often parameterized by empirical corrections to the surface layer similarity functions for conditions of strong stability (Holtslag and de Bruin 1988; Beljaars and Holtslag 1991). Furthermore for very stable situations, these empirical corrections are needed to prevent a decoupling of the atmosphere in NWP resulting in too-low surface temperatures (Louis 1979; Beljaars and Viterbo 1998). The decoupling phenomenon is closely related to intermittency, because of the fact that this decoupled system can become recoupled again by the influence of increased shear forced by the pressure gradient, leading to intermittent turbulence at the surface (Derbyshire 1999). Later in this text, we will discuss the effect of such empirical corrections on SBL model behavior with respect to the intermittency phenomenon.

The purpose of this paper is to show that the main mechanism behind ASI can be described with a simple, nonlinear bulk model, consisting of a coupled system of three nonlinear differential equations. This model mimics oscillatory SBL behavior triggered by the interaction between the bulk of the SBL and the underlying surface. Turbulence interactions with the overlying atmosphere are ignored. The bulk model appears to describe the main features of the oscillatory SBL. The main advantage of this approach is that it allows analytic solutions, which (a) give more insight in the influence of external (synoptic) forcings on the SBL development and (b) give more insight in the internal system dynamics of the complex interactions between the radiation and turbulent processes.

The results of our approach are described in two papers: in part I the model is described and several numerical solutions are presented, showing different regimes of behavior. In a companion paper (hereafter denoted as Part II), analytic solutions will be presented. Herein, it will be shown that the numerical results can be generalized in such a way that the occurrence of intermittent turbulence can be predicted from the evaluation of external parameters such as pressure gradient, cloud cover, and surface roughness (an extended abstract based on both papers is given in Van de Wiel et al. 2000).

In section 2 the model equations are given. In section 3 typical examples of the model dynamics are given. The effect of different turbulence parameterizations on the model outcome is discussed in section 4. Section 5 deals with the comparison of our results with earlier studies. Finally, conclusions of this work are presented in section 6.

2. Model setup

a. General description

Points of departure for the current model of the physics in the SBL are the conservation equations for momentum and heat. In the derivation of the model equations, it is our aim to reduce the complexity of the physical system to a minimum while preserving those physical processes which, according to the authors, are the most relevant to study the present mechanism. In connection with this aspect, Derbyshire (1999) argues that even the simplest analysis needs to couple explicitly the wind profile, temperature profile, and surface-heat budget. As shown below, our model design is in compliance with this statement. Furthermore, in section 3a, we will show that the model behavior of this simplified model resembles the behavior of more detailed models.

We designed our atmosphere–surface bulk model with the following features:

1) It describes the interaction between the "bulk" of the SBL and the underlying surface.
2) The surface is covered with a low vegetation layer.
3) There is no interaction (except for radiation) between the turbulent SBL and the "free" atmosphere above: at the top of the SBL the fluxes of momentum and sensible heat are zero.
4) The depth of the SBL is taken constant (see section 2e).
5) The SBL is "dry;" that is, phase changes of water variables are ignored and there is no surface evaporation.
6) It is a bulk model; that is, only the time evolution of the depth-averaged temperature and wind speed is considered.
7) A simple radiation scheme is used based on a quasi-gray body approach for the longwave radiation emitted and absorbed by the SBL, the surface and the overlying "free" atmosphere, and clouds.
8) In the momentum equation, the Coriolis force is neglected.

The third and eighth assumptions, above, are discussed in more detail because they limit the applicability of the model results. Several observational studies (e.g., Caughey et al. 1979; Mahrt et al. 1979; Nieuwstadt 1984) of the SBL show a decrease of the turbulent fluxes with height. In those cases, the height at which the fluxes vanish is referred to as the boundary layer depth. The present study is applicable to this type of condition where there is no turbulent transport between the turbulent SBL and the "free" atmosphere above. Basically, the restriction to these special cases was made in order to limit the complexity of the model (see Part II). This restriction means that the present model cannot be applied in situations where the turbulence intensity increases with height. These kinds of stable "boundary layers" are also commonly observed [e.g., Smedman (1988) and recent observations during CASES99 by L. Mahrt (2001, personal communication); for a review of these so-called "top-down boundary layers," see Mahrt (1999)]. Obviously, this kind of top-down transport may influence SBL dynamics (McNider et al. 1995; Vukelic and Cuxart 2000; also see discussion in section 5a).

Therefore, in the future, the present analysis could be generalized by including this type of interaction.

The eighth assumption considers the fact that the Coriolis force acts on the SBL with a timescale of a few hours [e.g., 3 h at 45° latitude; Blackadar (1957)], whereas the dynamics of the intermittent turbulent boundary layer have a typical timescale in the order of 1 h (Revelle 1993). Furthermore, comparison of the present model with the results of Revelle (1993), who included Coriolis effects, reveals that Coriolis effects are not essential for the intermittency mechanism to occur. The consequence of this assumption is that, in the present study, our pressure gradient term is, in fact, the ageostrophic (or effective) pressure gradient term. In other words, it is the pressure gradient in the direction of the mean flow. This, has to be kept in mind when interpreting the results.

Our physical model, sketched in Fig. 2, consists of four layers:

- The (deep) soil, which is kept at a constant temperature, T_M; $-\infty < z < 0$.
- The vegetation layer with depth d; $0 \leq z \leq d$. [Within this layer, at the bottom of the vegetation layer, a thin mulch layer with thickness δ_m is present, which is regarded as a resistance, not as a separate layer (see section 2e).]
- The air layer, which has a constant depth h (the actual SBL); $d < z \leq h$.
- The free atmosphere above the SBL (the longwave radiation emitted by the free atmosphere does not vary in time); $h < z < \infty$.

For this system, the basic equations for the layered averaged wind speed $\langle U \rangle$, air temperature $\langle T_a \rangle$ and vegetation temperature $\langle T_s \rangle$ are given by (see appendix A for list of symbols),

$$\int_d^h \frac{\partial U}{\partial t} \, dz = h \frac{\partial \langle U \rangle}{\partial t} = -\frac{h}{\rho} \frac{\partial P}{\partial s} + \frac{1}{\rho}(\tau_h - \tau_0), \qquad (1)$$

$$\int_d^h \frac{\partial T_a}{\partial t} \, dz = h \frac{\partial \langle T_a \rangle}{\partial t}$$

$$= \frac{1}{\rho c_p}(R_h - R_0) - \frac{1}{\rho c_p}(H_h - H_0), \quad \text{and} \quad (2)$$

$$\int_0^d \frac{\partial T_S}{\partial t} \, dz = d \frac{\partial \langle T_s \rangle}{\partial t} = -\frac{1}{\rho_v c_v}(G_d - G_0). \qquad (3)$$

Equation (1) represents the conservation of momentum for the depth-integrated SBL. The first term represents the pressure gradient, an external variable determined by large-scale atmospheric processes. As before, this term represents the pressure gradient in the direction of the mean wind (the effective pressure gradient). The second term is the friction at the top and the bottom of the SBL. The second and the third expressions are the energy conservation equations for the SBL and the vegetation layer. Herein H stands for the
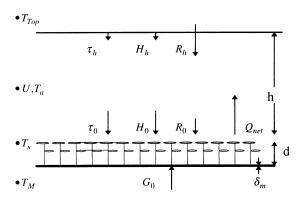

FIG. 2. The model system: state variables, fluxes, and model domain. (See appendix A for list of symbols.)

turbulent heat flux and R for the net longwave radiation for the *air layer* at the top and the bottom of the SBL. Parameters G_d and G_0 represent the energy flux at the vegetation top and the soil heat flux respectively. Note that $G_d = -Q_{net} + H_0$, with Q_{net} the net longwave radiation at the vegetation top (Q_{net} positive downward; G_d, H_0 positive upward). In the next sections, a more detailed description of the various process parametrizations are given. The detailed model equations are summarised in appendix B.

b. Parameterization of turbulent fluxes

To solve Eqs. (1)–(3) the turbulent fluxes at the boundaries of the atmospheric layer $z = 0$ and $z = h$ are required. In our model we assume the turbulent fluxes vanish at $z = h$, which means $\tau_h = 0$ and $H_h = 0$. The turbulent fluxes at the boundaries are parameterized in terms of bulk properties of the SBL; that is, a drag law formulation is applied. Although, in literature, a variety of drag law formulations are available (Csanady 1967; Blackadar and Tennekes 1968; Yamada 1976; Louis 1979), the universality of drag laws is still under question (Stull 1990). Especially at high stabilities when fluxes are not constant with height and nonstationary effects are present, those kinds of flux parameterizations can be debatable (Delage 1997). Nevertheless, in our opinion, it is useful to adopt a drag law formulation as a first-order approximation to account for the basic feedback mechanisms between stratification, shear and turbulence. Therefore a drag law is chosen considering the following aspects:

- The drag law should possess the strong feedback mechanism of stability on turbulent mixing efficiency (i.e. dependent on some form of Ri number).
- The drag law should match with the integrated surface layer profiles resulting from similarity theory.

Also, for the purpose of our analytical analysis (Part II), the drag law formulation should be as simple as possible. As a matching case, the similarity functions of Businger et al. (1971), based on extensive surface layer

measurements, are chosen. This results in a drag coefficient (or turbulent exchange function) that is quadratically dependent on the bulk Richardson number, assuming a critical value of the latter of 0.2 (see section 3c; McNider et al. 1995; Derbyshire 1999). The surface layer fluxes thus are calculated as,

$$\tau_0 = \rho u_*^2 = \rho \langle U \rangle^2 \cdot \frac{\kappa^2}{\left[\ln\left(\frac{\tilde{h}}{z_0}\right) \right]^2} \cdot f(R_b); \qquad (4)$$

$$H_0 = -\rho c_p \cdot |\langle U \rangle| \cdot \Delta T \cdot \frac{\kappa^2}{\left[\ln\left(\frac{\tilde{h}}{z_0}\right) \right]^2} \cdot f(R_b), \qquad (5)$$

where

$$\Delta T = \langle T_a \rangle - \langle T_s \rangle,$$

$$R_b = (\tilde{h} - z_0) \cdot \frac{g}{T_{\text{Ref}}} \cdot \frac{(\langle T_a \rangle - \langle T_s \rangle)}{\langle U \rangle^2}; \quad \text{and}$$

$$f(R_b) = \left(1 - \frac{R_b}{R_c} \right)^2; \qquad 0 \le R_b \le R_c$$

$$f(R_b) = 0; \qquad R_b > R_c. \qquad (6)$$

A reference height $\tilde{h}$ has to be chosen, which is representative for the SBL profiles. In situations with intermittent turbulence and oscillating mean variables, SBL profiles will be time-dependent, causing the reference height to be a function of time. For simplicity, an effective reference height, representing the bulk of the SBL is defined, arbitrarily set at $h/2$. Furthermore, in the model we assumed that $Z_{0m} = Z_{0H} = Z_0$. For notational convenience $\langle U \rangle$, $\langle T_a \rangle$, and $\langle T_s \rangle$ will be replaced in the following by U, T_a, and T_s.

c. Parameterization of longwave radiation

In the model, a so-called "emissivity approach" is adopted to describe the radiative characteristics of the atmosphere. It is well-known that the lower atmosphere does not emit or absorb longwave radiation in the frequency range 8–14 μm, known as the atmospheric window (Paltridge and Platt 1976), and that it is almost opaque outside this region. Therefore an apparent emissivity is assigned to the lower atmosphere with a value in the range 0.7–0.9. Also clouds play an important role in the nocturnal surface radiation budget, because they emit longwave radiation both outside and inside the atmospheric window range. This extra amount of radiation is not absorbed by the air, but (almost) totally absorbed by the surface. Although this extra radiative forcing, strictly speaking, depends on the cloud cover, type, and height of the clouds, a first-order approximation only depending on cloud cover was adapted to simulate this effect: cloud$^\downarrow = N \cdot 60$ W m^{-2} (low-level clouds at midlatitudes; Paltridge and Platt 1976).
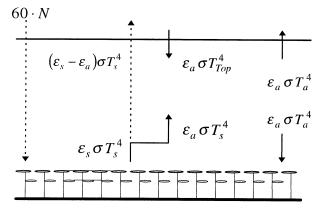

FIG. 3. Overview of model longwave radiation components.

For the vegetation surface the radiative budget reads (Fig. 3)

$$Q_{\text{net}} = \varepsilon_a \sigma T_a^4 + N \cdot 60 - \varepsilon_s \sigma T_S^4. \qquad (7)$$

From the amount of longwave radiation emitted by the surface, only a part—$\varepsilon_a \sigma T_S^4$ (W m^{-2})—is absorbed by the overlying air layer. The remaining part of the surface radiation (i.e., the part emitted in the window range) leaves the system.

Thus, the radiative budget for the air layer reads

$$R_h - R_0 = (\varepsilon_a \sigma T_{\text{Top}}^4 - \varepsilon_a \sigma T_a^4) - (\varepsilon_a \sigma T_a^4 - \varepsilon_a \sigma T_s^4), \quad (8)$$

assuming the same emissivity for the air layer and the overlying air.

Next, for simplicity and for the purpose of our analytical analysis of the system equations (see Part II) these equations will be linearized near a reference temperature by applying a Taylor series expansion, which leads to radiation terms linear in T_a and T_s. The linearized radiative budget for the air layer reads

$$R_h - R_0 = 4\varepsilon_a \sigma T_{\text{Ref}}^3 (T_s + T_{\text{Top}} - 2T_a). \qquad (9)$$

The linearized radiative budget for the vegetation surface reads

$$Q_{\text{net}} = [-\sigma(\varepsilon_s - \varepsilon_a) T_{\text{ref}}^4 + N \cdot 60] + 4\varepsilon_a \sigma T_{\text{ref}}^3 (T_a - T_s)$$

$$- 4\varepsilon_a \sigma T_{\text{ref}}^3 \left(\frac{\varepsilon_s}{\varepsilon_a} - 1 \right) \cdot (T_s - T_{\text{ref}}). \qquad (10)$$

The first term on the right side will be defined as the isothermal net radiation:

$$Q_i = -\sigma(\varepsilon_s - \varepsilon_a) T_{\text{ref}}^4 + N \cdot 60. \qquad (11)$$

This isothermal net radiation is defined as the net radiation that would occur under isothermal conditions. It depends on the radiative properties ε_s, ε_a, and N of the atmosphere and the vegetation cover, and determines the maximum radiative forcing on the system. It is comparable with the isothermal net radiation as defined by Monteith (1981) and by Holtslag and De Bruin (1988). For example, under cloudless conditions with ε_a equal

TABLE 1. Overview of model parameters and physical constants. The values given are used in the model runs, unless stated otherwise. (Int. and ext. refer to internal and external variables/parameters, respectively; phy. is for physical.)

Symbol	Description	Type	Value (reference)	Units
U	Wind speed	Int. variable	Variable	$(m\ s^{-1})$
T_a	Air temperature	Int. variable	Variable	(K)
T_s	Surface temperature	Int. variable	Variable	(K)
$\dfrac{1}{\rho}\dfrac{\partial P}{\partial s}$	Effective pressure force (per mass)	Ext. parameter	2.0×10^{-4}	$(m\ s^{-2})$
N	Cloud fraction	Ext. parameter	0.0	(—)
z_0	Roughness length	Ext. parameter	0.05	(m)
ε_a	Air emissivity	Ext. parameter	0.78	(—)
ε_s	Surface emissivity	Ext. parameter	1.0	(—)
C_v	Heat capacity (per m²) of low vegetated surface	Ext. parameter	2000	$(J\ m^{-2}\ K^{-1})$
λ_m/δ_m	Bulk conductance of mulch/stagnant air layer	Ext. parameter	2.5	$(W\ m^{-2}\ K^{-1})$
T_{ref}	Reference temperature	Ext. parameter	285	(K)
h	Boundary layer height	"Int./ext." par. (see section 2e)	80.0	(m)
$\tilde{h}$	Reference height ($h/2$)	"Int./ext." par. (see section 2e)	40.0	(m)
c_p	Heat capacity of dry air (at constant pressure)	Phys. constant	1005	$(J\ kg^{-1}\ K^{-1})$
ρ	Density of dry air	Phys. constant	1.2	$(kg\ m^{-3})$
R_c	Critical bulk Richardson number	Phys. "constant" (see section 3e)	0.2	(—)
g	Gravity constant	Phys. constant	9.81	$(m\ s^{-2})$
κ	von Kármán constant	Phys. constant	0.4	(—)
σ	Boltzmann's constant	Phys. constant	5.67×10^{-8}	$(J\ K^{-4}\ s^{-1})$

to 0.8, and ε_s equal to 1.0 this would result in a Q_i of -75 W m^{-2}, which is a typical value of the isothermal net radiation under those conditions.

d. Parameterization of surface temperature dynamics

In our model the surface temperature dynamics are described by a simple soil–vegetation scheme. It is well-known that the existence of a small (isolating) vegetation layer has a large impact on the development of the nocturnal surface temperature (Duynkerke 1999). In case vegetation is present, the direct influence of the soil heat flux on the energy balance of the vegetation top is limited. This effect results in much lower surface temperatures for grassland than for bare soils or road surfaces (Best 1998). Also, because of this limited interaction and because of the *small thermal inertia* of the vegetation layer, the vegetation temperature is able to respond to quickly varying external forcings (Acevedo et al. 2000). This rapid reaction of the surface temperature has a direct impact on the stability of the lower atmosphere, which, in turn, has important consequences for the near-surface atmospheric dynamics. Of course, this is particularly valid for situations with intermittent turbulence. However, the influence of this sensitivity of the vegetation temperature is not always considered in modeling studies, because often the (slow) diurnal cycle is studied.

Our soil–vegetation system consists of a thin vegetation layer with a small heat capacity. At the bottom of this vegetation layer there is a thin, loose organic mulch layer formed from dead plant material. Further we assume that

1) the soil layer has a constant temperature (i.e., the resistance of the mulch layer with nonturbulent air is large compared to the resistance to heat transport in the soil), and
2) heat within the small canopy is distributed instantaneously within the canopy, so that the vegetation temperature is approximately equal to the vegetation surface temperature.

Thus the heat budget of the vegetation layer is (cf. Duynkerke 1999)

$$\frac{\partial T_S}{\partial t} = \frac{1}{C_v}\left[Q_{net} - H_0 - \frac{\lambda_m}{\delta_m}(T_S - T_M)\right], \quad (12)$$

where T_s is the vegetation temperature, T_M is the soil temperature, and δ_m and λ_m are the thickness and conductivity of the mulch layer. It is noted that value of the bulk conductance (defined as λ_m/δ_m) of the mulch/air layer in the vegetation (2.5 W m^{-2} K^{-1}; Table 1) is comparable with the value reported by Duynkerke (1999; 3 W m^{-2} K^{-1}), estimated from Cabauw measurements over short grass. Parameter C_v stands for the heat capacity of the vegetation per unit of area (J K^{-1} m^{-2}) ($C_v = \rho_v c_v d$; see symbol list).

Note that the mathematical structure of (12) is such, that, by using different parameters, it exactly describes

the surface temperature dynamics of a homogeneous (bare) soil, according to the well-known force–restore method (Deardorff 1978). In section 3e this bare-soil interpretation of the problem will be addressed.

e. Model equations and solving

The final model consists of the set of equations that is given in appendix B. This set, derived in the previous sections, describes the development of the air temperature, the surface temperature and the wind speed in time. The equations are integrated in time using a fourth-order Runge–Kutta technique with a time step of 10 s. The time integrations proved to be numerically stable for all runs. It is noted that, except for the example in section 3a, only *stationary situations* are considered. This was done to enable a direct comparison between the present numerical results and the analytical analysis (Part II), which is valid for the equilibrium situation. On average, stationarity is reached within 15 h, depending on the initial conditions and the thermal properties of the atmosphere and of the surface. To be sure about stationarity, runs after 30 h are shown. In advance, it is noted that, in general, the dynamic model behavior (the intermittency) does not differ much between the transient period and the stationary period, enabling a possible extension of the stationary results to more realistic (i.e., transient) cases (see section 5).

The model variables T_a, T_s, and U are referred to as *internal variables,* because they are time-dependent and consequently have a range of values for one run in time. It is noted that the bulk-Richardson number—which is directly related to T_a, T_s, and U—is also a time-dependent internal variable. On the other hand we will denote surface roughness, surface and air emissivity, cloud cover, and pressure gradient as *external parameters.* These parameters, *which are constant* in time for each run, determine the development of the internal variables. So the physical behavior simulated by the model will depend on the actual values of the external parameters. In Table 1 the values of the parameters and constants used in the model runs are given. Unless stated otherwise, the results shown have been obtained with these values.

In Table 1 the boundary layer height h is referred to as an external variable, because in our bulk model a fixed a priori value was assigned to the boundary layer height. This is in order to avoid model complexity for our analytical analysis. In a real SBL this parameter is part of the system itself, and thus a dependent internal variable. As a model extension, one might think of parameterizing this height as a relaxation process in terms of external variables such as pressure force and radiative forcing (cf. Nieuwstadt and Tennekes 1981).

3. Model results

a. Transient behavior

An example of a 10-h transient run is shown in Fig. 4, which is compared qualitatively with the results of
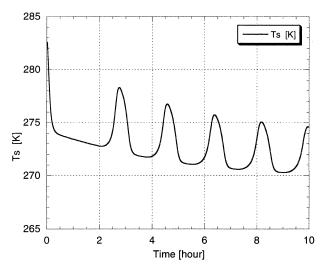

FIG. 4. Transient run showing the time evolution of the surface temperature during 10 h as calculated by the model.

an earlier study (not shown in Fig. 4) by Revelle (1993). Revelle uses a one-dimensional model with the same type of turbulence closure as in the present model. The model differs from the present model by the fact that it consists of a multilevel discretization, instead of a single level discretization and that it incorporates Coriolis effects, whereas in the present study these effects are neglected. In Fig. 4 a general decrease in surface temperature is seen as is generally observed in nocturnal conditions. Also after some time, sudden increases in temperature are visible, which after a short time drop back to the general trend. The occurrence of such temperature peaks confirms the results of Revelle, who showed that these peaks were related to intermittent bursts of turbulence. The period of the temperature peaks of about 1½–2 h is comparable with the periods of temperature peaks reported by Revelle (i.e., 30–240 min). The peak height of 4–5 K agrees with the peak height of the near-surface temperature of about 5 K as in Revelle (see his Fig. 3). Thus, the truncated model presented here essentially shows the same type of behavior as the more complex model. It is noted that temperature peaks of the surface temperature with a magnitude of several degrees are quite commonly observed. Coulter and Doran (2000) for example observed a decrease and increase of surface temperature of about 4 K within 2 h during the CASES99 experiment. Acevedo (2000) reported a temporal increase (+3 K) in near-surface temperature and humidity during intermittent turbulence bursts.

Thus, the example in Fig. 4 shows that, the intermittency mechanism described qualitatively in the introduction, can be captured by a system of three coupled nonlinear differential equations. Therefore, more insight into the ASI can be gained by studying the dynamics of this simplified system. In the next sections and in the
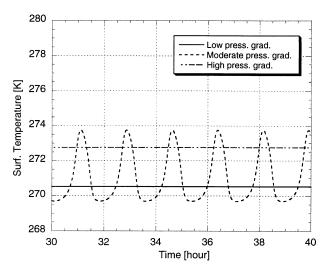
FIG. 5. Variation of surface temperature T_s after 30 h (equilibrium situation) for different values of the pressure gradient $-(1/\rho \cdot \partial P/\partial s)$.

companion paper (Part II) the behavior of the system will be studied in more detail.

b. Flow regimes

In this section different model regimes are studied as a function of the imposed effective pressure gradient. The pressure gradient is of importance in the SBL because it provides mechanical energy favoring turbulent mixing. Together with the amount of radiative surface cooling this turbulent mixing determines the strength of the nocturnal inversion (e.g., André and Mahrt 1982). In the following it will be shown that not only the inversion strength (mean state) of the SBL, but also the *dynamic behavior* is strongly influenced by this pressure gradient. In Fig. 5 the equilibrium value of the surface temperature is shown for three cases with different pressure gradients. Clearly, three different regimes are visible.

1) Weak (low) pressure gradient force: turbulent fluxes are weak, resulting in the lowest surface temperature corresponding to the strongest inversion. The solution has a nonoscillatory character.
2) Strong pressure (high) gradient force: turbulent fluxes are strong, resulting in the highest surface temperature corresponding to the weakest inversion. Again, the solution has a nonoscillatory character.
3) Moderate pressure force: turbulent fluxes are alternately weak and strong, resulting in intermediate, but strongly oscillating surface temperatures (for a qualitative physical interpretation, see introduction).

The existence of three different regimes agrees with the results of more complex models reported by Lin (1990) and Revelle (1993). The three regimes are a result of a strong interplay between various coupled physical processes:

- Wind speed is a function of the surface roughness, the pressure force and the stratification strength.
- The strength of the stratification is a function of the emissivities of the atmosphere (including clouds) and the land surface, and of the turbulent heat flux that, in turn, is an implicit function of wind speed.

There is a further discussion on the physical interpretation of the equilibrium system behavior in a companion paper.

c. The oscillatory regime

In this section the oscillatory case of the previous section is studied in more detail. In Fig. 6a the temporal behavior of the internal model variables U, T_a, and T_s is shown. The pattern of T_s, showing strong oscillations is the same pattern as presented in Fig. 5. Contrary to T_s, this oscillatory behavior has almost disappeared in the graph of T_a. This is not surprising, because of the fact that the integrated air layer has a relatively large heat capacity, so that the impact of the (relatively small) intermittent fluxes is largely damped out. The height-averaged wind speed clearly shows oscillatory behavior with amplitude of about 1 m s^{-1}. The wind speed increases during the quiet periods and decreases during the turbulence bursts conforms to the mechanism described in the introduction.

In the introduction it was argued that the oscillatory behavior of the mean variables like temperature and wind speed can be generated by intermittent turbulence (that is, discontinuous, but regular). This is illustrated in Fig. 6b, which corresponds to the same case as Fig. 5a. It is shown that the turbulent fluxes have a regular intermittent character leading to an oscillatory behavior of the mean variables. Also, for the intermittent case, the transport of turbulent heat flux (peak values of -33 W m^{-2}) and momentum flux (peak values of 0.25 m s^{-1}) is well correlated, in contrary to transport by linear gravity waves (e.g., Kondo et al. 1978). This coupled transport of heat and momentum is controlled by the dynamics of the bulk Richardson number, which strongly influences the mixing efficiency of turbulence, via the turbulence exchange function $f(R_b/R_c)$ (see Fig. 6c). In most cases (not shown here), the maximum value of (R_b/R_c) exceeded the value 1, resulting in periods with no turbulent transport, alternating with turbulent bursts. In some intermittent cases however, (R_b/R_c) did not cross the value of 1, which means that during intermittent turbulence the flow does not need to become completely laminar during calm periods, although it becomes very weakly turbulent. Thus Fig. 6c is an in-between case with R_b/R_c hardly exceeding 1.0. With respect to the discussion above it is noted that we adopted $(R_b/R_c) < 1$ (with R_c equal to 0.2 for the reasons explained in section 2b) as a *sufficient* condition for the onset of turbulence, using an empirical bulk Richardson number rather than a gradient Richardson number. Gen-
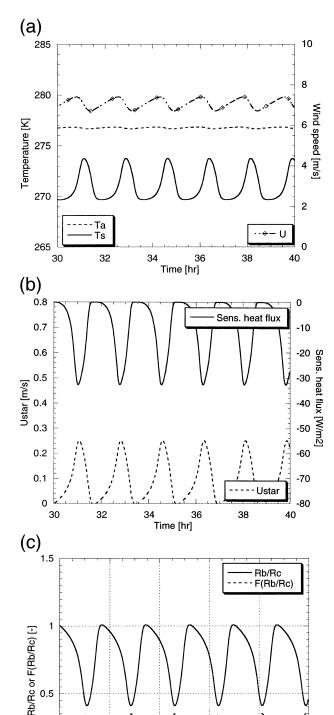
TABLE 2a. Amplitude of surface temperature T_s as a function of external forcing parameters $-(1/\rho \cdot \partial P/\partial s)$, N, and ε_a. The bold numbers represent the reference values from Table 1.

Parameter					
$-1/\rho \cdot \partial P/\partial s$ $(\times 10^{-4})$ (m s^{-2})	0.5	1.0	**2.0**	4.0	8.0
Amplitude T_s (K)	0	3.1	4.1	3.3	0
N (—)	**0.00**	0.25	0.50	0.75	1.00
Amplitude T_s (K)	4.1	2.9	0.8	0	0
ε_a (—)	0.70	**0.78**	0.82	0.86	0.90
Amplitude T_s (K)	5.9	4.1	3.0	1.5	0

erally, the theoretical condition $(R_i/R_c) < 1$ is only a *necessary* condition for the onset of turbulence [with R_c equal to 0.25; Miles (1961)].

d. Sensitivity to forcing parameters

In this section the sensitivity of the model to different atmospheric forcing parameters is investigated. In a companion paper (Part II) the results of sections 3d and 3e are generalized by introducing a dimensionless parameter from which the model behavior can be predicted.

In Table 2 a few forcing parameters are varied compared to their reference value (shown in bold in Table 2; only a single parameter is varied at a time). The amplitude of the equilibrium surface temperatures are given, with zero amplitude corresponding to the nonoscillating cases. In Fig. 5 it was shown that the value of the pressure gradient has a large influence on the different model regimes. This fact can also be found in Table 2 which shows no surface temperature amplitude at very low and high values of the pressure gradient, and large amplitudes at moderate pressure gradients. At the same time, it can be seen intermittent turbulence is more readily expected in situations with high radiative forcing, that is, low values of cloud cover (N) and atmospheric emissivity (ϵa) (Table 2). This follows the intuitive perception that no intermittency is expected under near-neutral stability conditions. Thus, it is concluded that intermittent turbulence is expected to occur during nights with clear skies in the presence of moderate to rather small pressure gradients.

e. Sensitivity to local surface parameters

The relation between intermittency and land surface characteristics is studied by investigating the sensitivity of the model to local surface parameters (Table 3). From Table 3 it can be seen that both the heat capacity of the vegetation layer and the bulk conductance (here defined as λ_m/δ_m) of the thin mulch–nonturbulent air layer are important parameters controlling the amplitude of the vegetation temperature: a vegetation layer with a small heat capacity and a low conductance to the upper soil is able to respond quickly to changing external forcings allowing a rapid change of stability in the lower atmosphere.

FIG. 6. (a) Behavior of the surface temperature T_s, air temperature T_a, and the wind speed U in a situation with intermittent turbulence. (b) Behavior of the sensible heat flux and the friction velocity in a situation with intermittent turbulence. (c) Behavior of the normalized bulk Richardson number R_b (R_b/R_c) turbulent exchange function $f(R_b)$, in an equilibrium situation with intermittent turbulence.

TABLE 2b. Amplitude of surface temperature T_s as a function of local surface parameters z_0, C_v, and λ_m/δ_m. The bold numbers represent the reference values from Table 1.

Parameter					
z_0 (m)	0.025	**0.050**	0.100	0.300	1.000
Amplitude T_s (K)	2.5	4.1	4.9	5.9	6.6
C_v (J m^{-2} K^{-1})	10 000	5000	**2000**	1000	500
Amplitude T_s (K)	0	0	4.1	6.9	8.7
λ_m/δ_m (W m^{-2} K^{-1})	10.0	5.00	**2.50**	1.25	0.625
Amplitude T_s (K)	0	0	4.1	6.6	8.3

Table 3 also shows that larger oscillations of surface temperature are expected over rough surfaces than over smooth surfaces. Thus, the results of Table 3 clearly show that the intermittent surface–atmosphere dynamics are very sensitive to the surface characteristics. This means that for this type of intermittency modeling, a rather detailed description of physical surface characterics is needed to model the rapid surface temperature fluctuations found in these circumstances.

In this light it is interesting to know what would happen above a bare soil surface or over an ocean. To look at this aspect we first point out the following: mathematically, Eq. (12), which describes the temperature development of a vegetation, is exactly equivalent to the well-known force–restore method. This method uses an analytical solution for a (single-mode) sinusoidal forcing on a homogeneous soil to describe the temporal evolution of the surface temperature (e.g., Deardorff 1978). According to this method, the equation for the surface temperature over a bare soil is given by:

$$\frac{\partial T_S}{\partial t} = \frac{2}{\rho_g c_g d_g}(Q_{\text{net}} - H_0) - \omega(T_S - T_M), \quad (13)$$

where ρ_g is the density (in kg m^{-3}) and c_g (in J kg^{-1} K^{-1}) is the heat capacity of the soil; $\omega(=2\pi/\text{period})$ (in rad s^{-1}) is the angular frequency of the external forcing and T_S (in K) and T_M (in K) are the surface and deep soil temperature, respectively. The so-called e-folding depth d_g (in m) depends on both the thermal properties of the soil as well as on the frequency of the imposed forcings:

$$d_g = \sqrt{\frac{2\lambda_g}{\omega \rho_g c_g}}, \quad (14)$$

where λ_g (in W m^{-1} K^{-1}) is the conductivity of the soil. The force–restore method is often applied for modeling the diurnal cycle of the surface temperature for which the period is known. This contrary to the present intermittent case, where this a priori choice is not evident. Based on our earlier results (section 3a) and on the results of Revelle (1993) periods of 30 min, 1½ h, and 4 h are used as a test case (in principle it is also possible to find the period in an iterative way). Model simulations were performed for three different soil types:

1) dry sand (λ_g = 0.30 W m^{-1} K^{-1}, ρ_g = 1.6 · 10^3 kg m^{-3}, c_g = 0.80 · 10^3 J kg^{-1} K^{-1}, and d_g = 0.012–0.033 m);

2) wet sand (λ_g = 2.2 W m^{-1} K^{-1}, ρ_g = 2.0 · 10^3 kg m^{-3}, c_g = 1.48 · 10^3 J kg^{-1} K^{-1}, and d_g = 0.021–0.058 m); and

3) clay (λ_g = 1.18 W m^{-1} K^{-1}, ρ_g = 1.8 · 10^3 kg m^{-3}, c_g = 1.25 · 10^3 J kg^{-1} K^{-1}, and d_g = 0.017–0.049 m).

The model results were the same for the different soil types: none of the soil types shows intermittent behavior. This is caused by the fact that the soil heat capacity and its conductivity are large compared to the vegetated case, which prevents a rapid surface cooling. Keeping in mind the limitations of the force–restore method it is concluded that, according to the present model, intermittency is not easily found above a homogeneous bare soil. Of course, inhomogeneous (e.g., crusted or tilted) soils will behave differently. Also, intermittency having *another origin* than the present mechanism, may still occur. We may extend these bare soil conclusions to oceans: due to the extremely large heat capacity of water it is likely that the intermittent surface–atmosphere dynamics will not occur above a large water surface.

4. Impact of turbulence parameterization

a. Stability functions

In this section we will investigate the effect of the turbulence parameterization on the model outcome by comparing different types of stability functions. In Fig. 7 a few examples of such stability functions are given as a function of the bulk Richardson number. The rationale behind these functions differs from one to another, reflected in the different shapes of the stability functions. The quadratic and the linear stability functions, for example, assume the existence of a critical (bulk) Richardson number, beyond which no turbulent transport is possible. This clearly results in a sharp cutoff of the stability function at this critical value of the bulk Richardson number. On the other hand, some of the other functions assume no critical bulk Richardson number resulting in a "broad tail" of the stability function. For example, the formulation of Beljaars and Holtslag (1991) allows some turbulence transport event at high Richardson numbers to account for nonstationary effects such as the occurrence of intermittent turbulence. The well-known Louis functions (Louis 1979) show broad tails resulting in relatively high values of
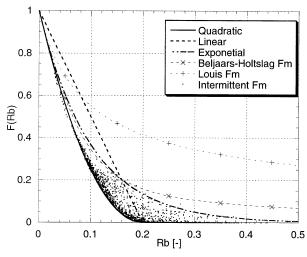
FIG. 7. Various stability functions for turbulent exchange as a function of the bulk Richardson number. The dots correspond to the *time-averaged* (30 min) values of the stability function during an intermittent run with the original quadratic stability function used in each time step.
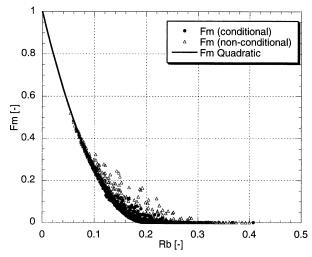

FIG. 8. Calculated stability functions $f_m(R_b)$ for oscillatory situations in the equilibrium, using conditional and nonconditional sampling. For comparison the original quadratic stability function used in the model is given.

the stability function at large R_b numbers. Although the Louis functions are not based on observational material, they are of great practical use in operational weather forecast models. They produce higher and more realistic surface temperatures in conditions of strong stratification, resulting in a better model performance than with the more observationally based stability functions (Beljaars and Viterbo 1998). This is related to the fact that modeling with the observationally based stability functions easily causes a decoupling of the atmosphere with the surface due to the small turbulent exchange at high stability (Beljaars and Holtslag 1991; Derbyshire 1999).

Finally, we mention the formulation of Mahrt (1987), that accounts for subgrid fluxes due to terrain heterogeneity. In this study only homogeneous situations are considered, which means that the Mahrt formulation does not apply. Nevertheless, considering the very broad tail of this stability function, it is likely that the results of Mahrt's functions would have been comparable with those of the Louis functions.

b. Modeled stability functions for the intermittent case

A novel and interesting result in Fig. 7 is given by the dots, which represent the time-averaged values of the stability function during a transient run with oscillations (as in Fig. 4), with the original quadratic stability function used instantaneously during each model time step. During the first 8 h of a transient run, half-hour averages of wind speed, temperature, and turbulent fluxes were calculated as is common practice in observational studies. From these half-hour fluxes and gradients, the mean Richardson number and stability functions f_m and f_h were calculated (only f_m is given in Fig. 7). We

observe that the explicit modeling of the intermittent turbulence is reflected in the (small) tail behavior of the stability function, although the original quadratic stability function shows no tail. This confirms the earlier statement that stability function with broad tails can be regarded to some extent as time-averaged parameterizations of intermittency and nonstationary effects. Also, due to the intermittent character of the turbulence, the uniqueness of the (averaged) flux profile relationship is gone. This is mainly due to the fact that the mean gradients are largely determined by the relatively long quiet period with little turbulence, while the fluxes are largely determined by the short bursting period. This means that a direct link between the flux and the gradient cannot exist.

By sampling at fixed times (as is common practice), extreme cases, such as 90% of the time interval with laminar flow and 10% turbulent flow, are easily included, causing large scatter in the time-averaged stability function (for reasons given above). This scatter can be reduced if one samples conditionally over a complete intermittent period (i.e., over both a laminar and a turbulent period), so that the time-averaged profiles and fluxes are more representative for the sampling period. In Fig. 8, stability functions are compared for the conditional and the nonconditional sampling case, calculated for the same equilibrium run. From this figure it is concluded that, by using conditional sampling, a better estimate of the "mean" gradients and fluxes during intermittent turbulence is made, resulting in a stability function that resembles more the original Businger–Dyer function. Of course, some scatter remains present, due to the "non uniqueness" of the flux profile relationships in intermittent conditions.

It is noted that in Fig. 8, other than in Fig. 7, the (bulk) Richardson numbers are calculated by dividing
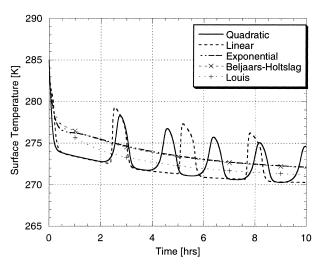
FIG. 9. Transient runs for different turbulent parameterizations $f_{m,h}(R_b)$, showing the time evolution of the surface temperature T_s during 10 h as calculated by the model.

the total buoyancy destruction [$\propto \Sigma (T_a - T_s)$] by the total shear production ($\propto \Sigma \, U^2$). This somewhat different averaging procedure is done because, strictly speaking, $\overline{U}^2 \neq \overline{U^2}$ for a nonstationary situation. The use of a different averaging procedure for the Richardson number, however, had very little effect on the results.

c. Transient runs for different stability functions

To investigate the effect of the shape of the stability functions on the SBL dynamics, 10-h transient runs of the surface temperature were generated and are plotted; Fig. 9 corresponding to the different stability functions showed in Fig. 7. For all runs, the same set of parameters given in Table 1 are used. It can be seen that the general decrease in surface temperature is comparable for the different parameterizations. On the other hand, for this particular set of parameters, oscillatory behavior with intermittent turbulence occurs for two stability functions only. Both oscillatory runs correspond to stability functions with a sharp cutoff, that is, stability functions that assume the existence of a critical Richardson number, beyond which no turbulent transport is possible. To investigate if the sharp cutoff in the stability function is responsible for the oscillatory behavior, a number of additional runs with the noncutoff turbulent parameterizations were carried out. It turned out that for these stability functions oscillatory solutions are also possible. For example, a run with the exponential stability function using different values of C_v (500 J m^{-2} K^{-1}) and roughness length (0.5 m), produces intermittent turbulence with oscillatory behavior in the surface temperature with a period of about 1 h. Using the same values and doubling the pressure gradient (8.0 · 10^{-4} m s^{-2}), the Beljaars–Holtslag functions also produce oscillatory behavior with a period of about half an hour. *Thus a sharp cutoff is not necessarily responsible for oscilla-*

tory behavior, which confirms the finding of Derbyshire (1999) stating that such a cutoff is not a necessary condition for SBL decoupling. On the other hand, multiple runs show that a broad tail in the stability functions is able to suppress oscillatory behavior, so that the set of physically realistic parameters causing oscillatory behavior becomes smaller for these type of functions. Thus a nonoscillatory solution is *more likely* when the stability function attains a limited value at high Ri numbers. Specifically the Louis formulation (1979) has such a broad tail that intermittency is not observed within the physically realistic parameter space. Thus, the use of broad-tail stability functions can be of practical use in numerical weather prediction, if one does not want to resolve oscillations.

5. Discussion

a. Comparison with previous work

The results from the numerical analysis with the one-layer model generally shows agreement with the behavior of the model results of Revelle (1993). Oscillating as well as nonoscillating regimes are encountered in both studies. It is worthwhile to note that, although a multilayered model up to 1 km is used by Revelle, the oscillating dynamics only occur in the lowest two model levels up to 10 m. His results show that at 30 m the atmosphere is decoupled from the surface and follows an inertial oscillation, as commonly observed in stable boundary layers (albeit mostly at higher levels). This is directly related to the fact that above 10 m the Richardson number is above the critical value. Revelle's use of two different values for the critical Richardson number for the surface layer (0.4) and the above surface layer (0.25) could have some influence, although it is noted by Revelle that a single Richardson criterion gives the same results for low geostrophic wind speeds (<5 m s^{-1}), that is, the range where the oscillatory behavior occurs. The fact that the oscillation dynamics only occur below 30 m in the example shown by Revelle, favors the use of a simple approach using a one-layer model in the present study.

Recently, an interesting study with different turbulence parameterization was carried out by Vukelic and Cuxart (2000). In their analysis they use an SBL model with a simplified second-order turbulence closure scheme [prognostic turbulent kinetic energy (TKE)] and apply constant surface forcing by prescribing the turbulent heat flux at the ground level. They show that oscillatory behavior (period of about 40 min) in the wind speed and the TKE production occurs in the upper part of the low-level jet. Because constant surface forcings are applied, they can not reproduce the intermittency, which was actually observed from measurements close to the ground. Instead, the model runs showed a ground level decoupled from the dynamics above.

Derbyshire (1999) reviews the decoupling phenom-

enon, which is defined as a cessation of turbulent transport between the surface and the atmosphere. In a situation with intermittent turbulence, also the surface layer itself temporarily becomes decoupled from the surface during quiet periods. So the decoupling process is closely related to the oscillatory behavior of turbulence as discussed in this text. Derbyshire shows that several SBL schemes seem to allow decoupling. Furthermore his analytical analysis, on a simplified Couette flow with no pressure force and Coriolis effects, shows that decoupling can be interpreted as a process driven by positive feedbacks between the surface temperature and the SBL parameterization, slowed down by soil thermal inertia. It is shown that the decoupling process is sensitive to the surface roughness and the soil thermal properties, which is confirmed by our results. Although in his article the possible recovery of the SBL (i.e., restored SBL–surface interaction) after a period of decoupling is not studied, Derbyshire mentions the importance of the large-scale pressure gradient on this SBL recovery (by acceleration leading to an increase of wind shear).

McNider et al. (1995) use a simplified, two-layer SBL model, with the same kind of parameterization as presented in this paper to study SBL dynamics. They report some oscillatory behavior of the mean variables for certain parameter ranges, which confirms the results of this study. Contrary to our results however, they report double-valued equilibrium solutions for certain values of the external parameters. For example two values of U_{eq}, $T_{a,eq}$, and $T_{s,eq}$ are found for a particular combination of external parameters. The existence of multiple solutions could have strong implications for the predictability of the SBL in the sense that even slight changes in initial conditions would lead to quite different solutions for temperature and wind speed. The difference in model behavior between both studies can be explained by the use of different boundary conditions. In our study at the upper model boundary the turbulent fluxes are assumed to be zero (prescribed fluxes). In the study of McNider et al. at the model boundary, the potential temperature and the wind speed (geostropic) are prescribed, allowing turbulent interaction between the actual model and the higher levels. Imposing this kind of boundary condition, two types of equilibrium solutions are basically possible: (1) the overlying air is decoupled from the model layer—in this case the equilibrium solution of the model basically follows our results, where the momentum of the model layer is supplied by the pressure force; and (2) the overlying air interacts with the model layer—in this situation extra momentum and heat from above are supplied to the model domain, resulting in an equilibrium solution different from the situation without this transport.

The numerical studies mentioned above show, that the basic intermittency mechanism, caused by the interaction between radiative cooling, pressure force, and the effect of stratification on turbulent mixing, is a possible candidate to be responsible for the observed in-

termittent behavior of the SBL. At the same time it is not clear at what level this intermittency is generated. Are the turbulent bursts generated close to the jet and transported downwards, or are they generated near the ground caused by the atmosphere–surface interaction (this paper)? It is clear that there is a need for experimental evidence (such as the CASES99 experiment; Poulos et al. 2000) that can provide more information about SBL dynamics, improving our knowledge about stable boundary layers.

b. Practical/experimental issues

In this study, a simple conceptual bulk model is developed to study SBL dynamics. Although such an approach has theoretical advantages, it requires special attention to practical/experimental issues. Due to the simplifications and assumptions, details are lost and results must be interpreted carefully. Below, some practical aspects are addressed that show why direct comparison of the model results with measurements is not straightforward:

- Most of the results, like the sensitivity analysis (Tables 2 and 3), were obtained for the equilibrium situation, which is reached no earlier than after 10–15 h, depending on the actual parameter values (section 2e). It is clear that most of the nocturnal boundary layers are not in equilibrium at all (e.g., Nieuwstadt et al. 1981). Therefore, for several runs, we compared the equilibrium model behavior with its transient behavior, with respect to the oscillations. It turned out that in most cases, the differences were only marginal, with slightly larger periods and amplitudes occurring in the transient period (e.g., compare Figs. 4 and 5).
- The assumption that the external parameters (e.g., pressure gradient and cloud cover) are constant during the night will be violated in practice (the same goes for the boundary layer height).
- Also, the assumption of horizontal homogeneity will be violated in practice. Not only synoptical parameters, but also surface characteristics vary in space. Without extending the present framework to 2D or 3D equivalents, the influence of inhomogeneity on intermittent surface–atmosphere dynamics can not be assessed.
- Although, predictions about the oscillatory behavior of the surface temperature can be easily verified, oscillations in the integrated values of mean variables will be more difficult to obtain: the values have small amplitudes and the height-integrated signal will be blurred by uncertainties in the SBL height estimations.

In addition, some important processes in the SBL such as dew/fog formation, advection, drainage flow and wave activity processes, are neglected. So in case the above-mentioned processes are important, the applicability of the model is limited. Nevertheless, in our opinion, this model could serve as a framework for future

theoretical and experimental research on this intermittency mechanism.

6. Conclusions

This paper focuses on an intermittency-generating mechanism that results from a *direct interaction between the lower atmosphere and the surface.* In this idealized case, interaction of the near-surface atmosphere with the low-level jet and/or elevated turbulence is not considered, despite their possible relevance to SBL dynamics. Also, the influence of other effects, often found in real SBLs, such as advection, gravity waves, drainage flows, and dew formation, is not considered. In future work, the present framework could be extended by incorporating these processes.

The main conclusion of this paper lies in the fact that this complex intermittency–atmosphere surface intermittency (ASI)—can be captured by a coupled system of only three nonlinear differential equations. This reduced system possesses the most essential elements of the SBL: buildup of stratification associated with a strong cooling of the surface by longwave radiation, supply of mechanical energy by the (ageostrophic) pressure gradient, and the limiting effect of stratification on turbulent mixing efficiency. It is also shown that both intermittent (oscillatory) and nonintermittent (nonoscillatory) regimes are found for different sets of external parameters. This result is confirmed by some others (e.g., Revelle 1993) with more detailed model configurations.

The reduction of the process complexity to a simple bulk system makes it possible to study this system analytically. In a companion paper an analytical system analysis is made, which leads to an explicit equilibrium solution of the system. By using analytical bifurcation theory the present numerical results are generalized such, that the occurrence of intermittent/oscillatory model behavior can be predicted from evaluation of the external parameters (see companion paper, Part II).

We found that intermittent turbulence is expected to occur in nights with clear skies in the presence of a moderate-to-rather-small (ageostrophic component of the) pressure gradient. Furthermore, it is found that the presence of a vegetation layer largely influences SBL dynamics. Due to the low heat capacity of the vegetation in combination with its isolating properties (stagnant air in the lower part of the canopy), its surface temperature may change rapidly on changing turbulent heat fluxes. This change in surface temperature in turn has a direct effect on the radiation and turbulent heat budgets, causing an important feedback mechanism, which may lead to instability (see Part II). According to the authors, any modelling of ASI should therefore include the possibility of a vegetation layer (or another isolating layer such as a snow layer). It was also found, that ASI is less likely to occur over bare soil surfaces, and unlikely to occur over large water surfaces, due to higher heat capacities and conductivity preventing rapid changes of surface temperatures.

A comparison on turbulence parameterization shows that the general shape of the stability functions (i.e., the limiting effect of stratification on turbulent mixing) is an important feedback mechanism in SBL modeling. In principle, a broad class of stability functions allow oscillatory behavior of SBL models. However, the shape of the tail of the stability functions plays an important role in suppressing this oscillatory behavior. Furthermore, it was shown that, in practice, a stability function with a sharp cutoff at the critical Richardson number *effectively* shows tail behavior when time averages are used. This is a consequence of averaging oscillatory, nonlinear processes, especially when nonconditional sampling is applied.

From the number of mechanisms that can cause an intermittent character of turbulence in the SBL, only one is considered in the present study. Currently, it is not clear if the different intermittency mechanisms are related to each other and where they occur in the SBL. For example, it is not clear whether turbulence bursts can be generated near the ground, or if they are generated near the low-level jet and transported downward. Therefore extensive experimental studies such as CASES99 (Poulos et al. 2000) are needed to clarify this issue and improve our knowledge about the stable boundary layer.

APPENDIX A
Symbol List

Symbol	Description	Units
c_g	Heat capacity of the soil	(J kg^{-1} K^{-1})
c_p	Heat capacity of air at constant pressure	(J kg^{-1} K^{-1})
C_v	Heat capacity of the surface vegetation per unit area	(J m^{-2} K^{-1})
c_v	Heat capacity of the vegetation (specific)	(J kg^{-1} K^{-1})
d	Depth of the vegetation layer	(m)
d_g	E-folding depth of the soil layer	(m)
δ_m	Thickness of the mulch layer	(m)
ε_a	Emissivity of the atmosphere	(—)
ε_s	Emissivity of the surface	(—)
f	Stability function (turbulence exchange function)	(—)
f_m	Stability function for the turbulent momentum flux	(—)
f_h	Stability function for the turbulent heat flux	(—)
G_d	Heat flux at the top of the vegetation layer	(W m^{-2})
G_0	Heat flux at the soil surface	(W m^{-2})
h	Depth of the turbulent layer [xxxxx (BL) height]	(m)
$\tilde{h}$	Reference height, here defined as $h/2$	(m)
H_h	Sensible heat flux at the boundary layer top	(W m^{-2})
H_0	Sensible heat flux at the surface	(W m^{-2})
κ	von Kármán constant	(—)
λ_g	Soil conductivity	(W K^{-1} m^{-1})
λ_m	Conductivity of the mulch layer	(W K^{-1} m^{-1})
N	Fraction of cloud cover	(—)
P	Pressure	(Pa)
Q_{net}	Net radiation budget of the surface	(W m^{-2})
Q_i	Isothermal net radiation	(W m^{-2})
ρ	Density of dry air	(kg m^{-3})
ρ	Density of the vegetation layer (bulk)	(kg m^{-3})
ρ_g	Density of the soil	(kg m^{-3})
R_b	Bulk Richardson number	(—)
R_c	Critical bulk Richardson number	(—)
R_h	Net longwave radiation of the BL at the boundary layer top	(W m^{-2})
R_0	Net longwave radiation of the BL near the surface	(W m^{-2})
σ	Boltzmann's constant	(W m^{-2} K^{-4})
s	Horizontal distance	(m)
τ_0	Surface shear stress	(N m^{-2})
τ_h	Shear stress at the boundary layer top	(N m^{-2})
t	Time	(s)
ΔT	Temperature difference ($T_a - T_s$)	(K)
T_a	Height-averaged air temperature	(K)
$\langle T_a \rangle$	Height-averaged air temperature	(K)
T_M	Soil temperature	(K)
T_{ref}	Reference temperature	(K)
T_s	Vegetation (surface) temperature	(K)
$\langle T_s \rangle$	Depth-averaged vegetation temperature	(K)
T_{top}	Temperature of atmosphere above the turbulent boundary layer	(K)
U	Height-averaged wind speed	(m s^{-1})
$\langle U \rangle$	Height-averaged wind speed	(m s^{-1})
u_*	Friction velocity	(m s^{-1})
ω	Angular speed of intermittency period	(s^{-1})
z	Height coordinate	(m)
z_0	Roughness length	(m)

APPENDIX B

Full Set of Equations

Given our discussion in section 2, the full set of equations is summarized as:

$$\frac{\partial U}{\partial t} = -\frac{1}{\rho}\frac{\partial P}{\partial s} - \frac{1}{h} \cdot \frac{\kappa^2}{\left[\ln\left(\frac{1}{2}h\middle/z_0\right)\right]^2} \cdot U^2 \cdot f(R_b),$$

$$\frac{\partial T_a}{\partial t} = \frac{4\varepsilon_a\sigma T_{\mathrm{ref}}^3(T_s + T_{\mathrm{Top}} - 2T_a)}{\rho c_p h}$$
$$- \frac{1}{h} \cdot \frac{\kappa^2}{\left[\ln\left(\frac{1}{2}h\middle/z_0\right)\right]^2} \cdot U \cdot (T_a - T_s) \cdot f(R_b), \quad \text{and}$$

$$\frac{\partial T_s}{\partial t} = \frac{-\sigma(\varepsilon_s - \varepsilon_a)T_{\mathrm{ref}}^4 + 60 \cdot N}{C_v} + \frac{4\varepsilon_a\sigma T_{\mathrm{ref}}^3}{C_v} \cdot (T_a - T_s)$$
$$+ \frac{4\varepsilon_a\sigma T_{\mathrm{ref}}^3}{C_v} \cdot \left(\frac{\varepsilon_s}{\varepsilon_a} - 1\right) \cdot (T_{\mathrm{ref}} - T_s)$$
$$+ \frac{\rho c_p}{C_v} \cdot \frac{\kappa^2}{\left[\ln\left(\frac{1}{2}h\middle/z_0\right)\right]^2} \cdot U \cdot (T_a - T_s) \cdot f(R_b)$$
$$- \frac{1}{C_v} \cdot \frac{\lambda_m}{\delta_m} \cdot (T_s - T_M),$$

where,

$$f(R_b) = \left(1 - \frac{R_b}{R_c}\right)^2 = \left[1 - \frac{1}{R_c}\frac{g\left(\frac{1}{2}h - z_0\right)}{T_{\mathrm{ref}}}\frac{T_a - T_s}{U^2}\right]^2;$$

$$0 \leq \frac{R_b}{R_c} \leq 1, \quad \text{and}$$

$$f(R_b) = 0; \qquad \frac{R_b}{R_c} > 1.$$

REFERENCES

Acevedo, O. C., and D. R. Fitzjarrald, 2000: Relating temporal and spatial structure of the nocturnal surface layer to landscape heterogeneity. Preprints, *14th Symp. on Boundary Layer and Turbulence,* Aspen, CO, Amer. Meteor. Soc., 596–599.

André, J. C., and L. Mahrt, 1982: The nocturnal surface inversion and influence of clear-air radiative cooling. *J. Atmos. Sci.,* **39,** 864–878.

Beljaars, A. C. M., and A. A. M. Holtslag, 1991: Flux parameterization over surfaces for atmospheric models. *J. Appl. Meteor.,* **30,** 327–341.

——, and P. Viterbo, 1998: Role of the boundary layer in a numerical weather prediction model. *Clear and Cloudy Boundary Layers,* A. A. M. Holtslag and P. G. Duynkerke, Eds., Royal Netherlands Academy of Arts and Sciences, 287–304.

Best, M. J., 1998: A model to predict surface temperatures. *Bound.-Layer Meteor.,* **88,** 279–306.

Blackadar, A. K., 1957: Boundary-layer wind maxima and their significance for the growth of nocturnal inversions. *Bull. Amer. Meteor. Soc.,* **38,** 283–290.

——, 1979: High-resolution models of planetary boundary layer. *Advances in Environmental Science and Engineering,* J. R. Pfafflin and E. N. Ziegler, Eds., Gordon and Breech, 50–85.

——, and H. Tennekes, 1968: Asymptotic similarity in neutral barotropic planetary boundary layers. *J. Atmos. Sci.,* **25,** 1015–1020.

Businger, J. A., 1973: Turbulent transfer in the atmospheric surface layer. *Workshop on Micrometeorology,* D. A. Haugeri, Ed., Amer. Meteor. Soc., 67–98.

——, J. C. Wyngaard, Y. Izumi, and E. F. Bradley, 1971: Flux-profile relationships in the atmospheric boundary layer. *J. Atmos. Sci.,* **28,** 788–794.

Caughey, S. J., J. C. Wyngaard, and J. C. Kaimal, 1979: Turbulence in the evolving stable boundary layer. *J. Atmos. Sci.,* **36,** 1041–1052.

Coulter, R. L., and J. C. Doran, 2000: Intermittent turbulence events observed with a sonic anemometer and minisodar during CASES99. Preprints, *14th Symp. on Boundary Layer and Turbulence,* Aspen, CO, Amer. Meteor. Soc., 622–625.

Csanady, G. T., 1967: On the ''Resistance Law'' of a turbulent Ekman layer. *J. Atmos. Sci.,* **24,** 467–471.

Deardorff, J. W., 1978: Efficient prediction of ground surface temperature and moisture, with inclusion of a layer of vegetation. *J. Geophys. Res.,* **83,** 1889–1903.

Delage, Y., 1997: Parameterising sub-grid scale vertical transport in atmospheric models under statically stable conditions. *Bound.-Layer Meteor.,* **82,** 23–48.

Derbyshire, S. H., 1999: Boundary-layer decoupling over cold surfaces as a physical boundary instability. *Bound.-Layer Meteor.,* **90,** 297–325.

Duynkerke, P. G., 1991: Observation of a quasi-periodic oscillation due to gravity waves in shallow radiation fog. *Quart. J. Roy. Meteor. Soc.,* **117,** 1207–1224.

——, 1999: Turbulence, radiation and fog in Dutch stable boundary layers. *Bound.-Layer Meteor.,* **90,** 447–477.

Ha, K.-J., and L. Mahrt, 2001: Simple inclusion of Z-less turbulence within and above the modeled nocturnal boundary layer. *Mon. Wea. Rev.,* **129,** 2136–2143.

Holtslag, A. A. M., and H. A. R. de Bruin, 1988: Applied modelling of the nighttime surface energy balance over land. *Bound.-Layer Meteor.,* **27,** 689–704.

Kondo, J., O. Kanechika, and N. Yasuda, 1978: Heat and momentum transfers under strong stability in the atmospheric surface layer. *J. Atmos. Sci.,* **35,** 1012–1021.

Lin, J. T., 1990: The effect of inertial and turbulence oscillations in the stable boundary layer and their role in horizontal dispersion. M.S. thesis, Dept. of Mathematics, University of Alabama in Huntsville, 82 pp.

Louis, J.-F., 1979: A parametric model of vertical eddy fluxes in the atmosphere. *Bound.-Layer Meteor.,* **17,** 187–202.

Mahrt, L., 1987: Grid-averaged surface fluxes. *Mon. Wea. Rev.,* **115,** 1550–1560.

——, 1989: Intermittency of atmospheric turbulence. *J. Atmos. Sci.,* **46,** 79–95.

——, 1999: Stratified atmospheric boundary layers. *Bound.-Layer Meteor.,* **90,** 375–396.

——, C. Heald, D. H. Lenschow, B. B. Stankov, and L. B. Troen, 1979: An observational study of the structure of the nocturnal boundary layer. *Bound.-Layer Meteor.,* **17,** 247–264.

McNider, R. T., D. E. England, M. J. Friedman, and X. Shi, 1995: Predictability of the stable atmospheric boundary layer. *J. Atmos. Sci.,* **52,** 1602–1614.

Miles, J. W., 1961: On the stability of heterogeneous shear flows. *J. Fluid Mech.,* **10,** 496–508.

Monteith, J. L., 1981: Evaporation and surface temperature. *Quart. J. Roy. Meteor. Soc.,* **107,** 1–27.

Nappo, C., 1991: Sporadic breakdown of stability in the PBL over simple and complex terrain. *Bound.-Layer Meteor.,* **54,** 69–87.

Nieuwstadt, F. T. M., 1984: The turbulent structure of the stable, nocturnal boundary layer. *J. Atmos. Sci.,* **41,** 2202–2216.

——, and H. Tennekes, 1981: A rate equation for the nocturnal boundary-layer height. *J. Atmos. Sci.,* **38,** 1418–1428.

Paltridge, G. W., and C. M. R. Platt, 1976: *Radiative Processes in Meteorology and Climatology.* Vol. 5, *Developments in Atmospheric Science,* Elsevier Science, 318 pp.

Poulos, G. S., D. C. Fritts, W. Blumen, and W. D. Bach, 2000: CASES-99 field experiment: An overview. Preprints, *14th Symp. on Boundary Layer and Turbulence,* Aspen, CO, Amer. Meteor. Soc., 618–621.

Revelle, D. O., 1993: Chaos and ''bursting'' in the planetary boundary layer. *J. Appl. Meteor.,* **32,** 1169–1180.

Smedman, A.-S., 1988: Observations of a multi-level turbulence structure in a very stable atmospheric boundary layer. *Bound.-Layer Meteor.,* **44,** 247–264.

Stull, R. B., 1990: *Introduction to Boundary Layer Meteorology.* Kluwer Academic, 670 pp.

Thorpe, A. J., and T. H. Guymer, 1977: The nocturnal jet. *Quart. J. Roy. Meteor. Soc.,* **103,** 633–653.

Van de Wiel, B. J. H., R. J. Ronda, A. F. Moene, H. A. R. De Bruin, and A. A. M. Holtslag, 2000: Intermittent turbulence and oscillations in the stable boundary layer: A system dynamics approach. Preprints, *14th Symp. on Boundary Layer and Turbulence,* Aspen, CO, Amer. Meteor. Soc., 593–595.

Vukelic, B., and J. Cuxart, 2000: One-dimensional simulations of the stable boundary layer as observed in SABLES99. Preprints, *14th Symp. on Boundary Layer and Turbulence,* Aspen, CO, Amer. Meteor. Soc., 579–580.

Welch, R. M., M. G. Ravichandran, and S. K. Cox, 1986: Prediction of quasi-periodic oscillations in radiation fogs. Part I: Comparison of simple similarity approaches. *J. Atmos. Sci.,* **43,** 633–650.

Yamada, T., 1976: On the similarity functions A, B and C of the planetary boundary layer. *J. Atmos. Sci.,* **33,** 781–793.